Advanced Materials Science and Technology Vol 4 Issue 2 2022
DOI: 10.37155/2717–526X–0402–5

ORIGINAL RESEARCH ARTICLE

Open Access

Omniscient Pte.Ltd.

Oxidative Dehydrogenation of Propane over Nanostructured Mesoporous $VO_x/Ce_xZr_{1-x}O_2$ Catalysts

Bao Agula[1,2], Minglei Sun[2], Shihang Liang[3], Yongsheng Bao[1], Meilin Jia[1], Feng Xu[4,*], Zhong-Yong Yuan[2,*]

[1]Inner Mongolia Key Laboratory of Green Catalysis, College of Chemistry and Environmental Science, Inner Mongolia Normal University, Hohhot 010022, China.
[2]Key Laboratory of Advanced Energy Materials Chemistry (Ministry of Education), School of Materials Science and Engineering, Nankai University, Tianjin 300350, China.
[3]State Key Laboratory of Catalytic Materials and Reaction Engineering, Research Institute of Petroleum Processing, SINOPEC, Beijing 100083, China.
[4]Tianjin Workstation, Technology Center of Shanghai Tobacco Group Co., Ltd., Tianjin 300163, China.

***Correspondence to:** Feng Xu, Tianjin Workstation, Technology Center of Shanghai Tobacco Group Co., Ltd., Tianjin 300163, China. Email: xfrong99@sina.com; Zhong-Yong Yuan, Key Laboratory of Advanced Energy Materials Chemistry (Ministry of Education), School of Materials Science and Engineering, Nankai University, Tianjin 300350, China. Email: zyyuan@nankai.edu.cn

Received: September 3, 2022; **Accepted:** December 22, 2022; **Published Online:** December 26, 2022

Citation: Agula B, Sun M, Liang S, Bao Y, Jia M, Xu F and Yuan ZY. Oxidative Dehydrogenation of Propane over Nanostructured Mesoporous $VO_x/Ce_xZr_{1-x}O_2$ Catalysts. *Advanced Materials Science and Technology*, 2022;4(2):049385. https://doi.org/10.37155/2717-526X-0402-5

Abstract: High-surface-area mesoporous $Ce_xZr_{1-x}O_2$ materials synthesized through a surfactant-assisted approach of nanocrystalline particle assembly are utilized as a promising support for VO_x-based catalysts. The catalytic properties of the resultant $VO_x/Ce_xZr1\text{-}_xO_2$ nanocatalysts are evaluated by the oxidative dehydrogenation of propane using a microreactor-GC system. It is indicated that the catalyst particles are on a nanoscale, having a mesoporous structure with uniform pore-size distribution and high surface area. The catalytic behavior of these mesoporous nanostructured $VO_x/Ce_xZr1\text{-}_xO_2$ catalysts for the oxidative dehydrogenation of propane reaction relies on the vanadia loading amount, the calcination temperature, the surface area and the Ce/Zr ratio of the supports, the particle size of active compounds, and the additional contribution to the propylene formation derives from the contribution of the catalytic dehydrogenation of propane under oxygen-lean conditions. The catalyst prepared with 8 wt% vanadia loading on $Ce_{0.2}Zr_{0.8}O_2$ exhibits high and stable catalytic performance in the oxidative dehydrogenation of propane reaction.
Keywords: $VO_x/Ce_xZr1\text{-}_xO_2$ catalysts; Mesoporous materials; Nanostructure; Oxidative dehydrogenation of propane; Vanadia species

1. Introduction

Propylene is a crucial raw material for a range of products such as polypropylene, acrolein, polyacrylonitrile, and acrylic acid. Studies on propylene from low-cost, abundant propane have been receiving significant attention on account of the growing demand for propylene. The direct dehydrogenation of propane (DHP) is one of the on-purpose propylene production technologies[1,2], successfully employed on an industrial scale, utilizing chromium-based catalysts with Al_2O_3 support and alkali metal promoters[3]. However, major challenges associated with this process are the thermodynamic deactivation and limitations, which significantly impact the catalyst properties and stability[4-6]. For instance, DeRossi and coworkers synthesized a series of Cr/ZrO_2 catalysts which exhibited higher catalytic activity compared to the identically synthesized Cr/SiO_2 catalysts and Cr/Al_2O_3[6,7]. Nevertheless, it was also revealed that an enhancement for the thermal durability to against the harsh reaction temperature and surface areas of those Cr/ZrO_2 catalysts were still required[6].

In contrast, oxidative dehydrogenation of propane (ODHP), using O_2 as cofeeding gas, can solve these problems. This succedaneous process is thermodynamically favored owe to the low process temperature and enhanced catalyst durability by the prevention of coke deposition. In addition, this process is neither bound by equilibrium nor endothermic, and thus has important advantages compared to the established DHP processes. Unfortunately, till now, a low selectivity towards propylene caused by the formation of undesirable by-products due to the deep oxidation of propane and propylene severely influence the industrial application[8,9]. The main cause of the selectivity limitation derives from the conversion-selectivity relationship: a rise of propane conversion results in a decrease in propylene selectivity. A considerable amount of work was carried out for the promotion of selectivity to propylene during the ODHP by different methods. It was reported that alkali metal additives could enhance the selectivity to propylene in the ODHP on MoO_3/TiO_2, V_2O_5/TiO_2[10,11], V_2O_5/Al_2O_3[12] and V_2O_5/SiO_2, V_2O_5/MgO[13-15] catalysts; the effect was explained by the modification of the acid–base properties of the catalysts with the alkalis. In the studies of Kondratenko and coworker, the ODHP reaction over VO_x/γ-Al_2O_3[16] and VO_x/MCM-41[17] catalysts indicated that the propylene selectivity could be boosted when replacing O_2 using N_2O, suggesting that the enhanced ODHP performance with N_2O resulted from the lower ability of N_2O to enable the re-oxidation of the reduced VO_x species, i.e., the reduction degree of catalyst in the presence of N_2O is higher than that in the presence of O_2[18]. When CO_2 was utilized as the oxidant, the propylene selectivity over a Ga-based catalyst was enhanced[19]. However, an understanding of the effect of the dehydrogenation of propane for the promotion of the selectivity to propylene during the ODHP under oxygen-lean conditions is still necessary to be solved clearly.

Different kind of support materials and catalysts have been investigated in the ODHP reaction to date. VO_x-based catalytic systems have been found to be one of the most active catalysts[20] on account of their capacity to easily alter the oxidation state of vanadium between +3 and +5 quite. Supported vanadium oxide catalysts are typically more selective than the unsupported bulk V_2O_5 materials due to the strong interactions between the VO_x species and the oxide support substrates (e.g., Al_2O_3, Nb_2O_5, TiO_2, ZrO_2 and SiO_2,)[21-26]. Previous work has reported that the interactions between the deposited vanadium oxides and oxide support materials determine the structure of the generated surface VO_x species[24]. It was found that dehydrated VO_x species on catalyst surface had [VO_4] coordination with one terminal V = O bond and the polymerization degree was different on different carriers. Besides, at high surface vanadium oxide ratio, crystalline V_2O_5 bulks also exist. The activity and selectivity of these catalysts depend a lot on the specific oxide support and the loading of vanadium oxide. Lemonidou and coworkers[25] investigated the ODHP over a series of VO_x-based catalysts with supported on ZrO_2, MgO, Al_2O_3 and TiO_2 as supports and found that the activity (moles of propane converted per gram of the catalyst) was prominently influenced by the type of support. The VO_x-based catalysts with different mesoporous supports have also been found to be selective and active for the ODHP process[17]. Mesoporous materials with high surface areas can promote the dispersion of the surface active VO_x species.

Generally, total oxidation reaction is the main use of

the CeO_2 containing materials in catalysis fields[27,28]. The capacity of oxygen storage and release on CeO_2 support can provide more oxygen for oxidation processes, resulting from the redox couple "Ce^{4+}/Ce^{3+}"[27,29]. Gong and coworkers have reported that the introduction of ZrO_2 to CeO_2 could effectively regulate the structure of the CeO_2 crystallite and could form a Ce-Zr-O solid solution, achieving a great promotion on the O_2 storage capacity of CeO_2, the thermal resistance, the redox property and highly dispersive metal compounds[30-32]. Chen and coworkers[33] minutely investigated the effects of different Ce/Zr ratios for the $Ce_xZr_{1-x}O_2$ catalysts. It was revealed that $Ce_{0.8}Zr_{0.2}O_2$ was the most texturally stable composition[32,34]. Besides, the catalytic behavior of CeO_2 support could be significantly modified by the introduction of the dopants with strong interact with the CeO_2 support[27,28]. The V-doping CeO_2 materials have stimulate great interests on the ODHP reaction[35,36]. Meanwhile, the catalytic performance relies significantly on plenty of factors, including the acid-base character, the redox properties and the chemical nature of the active oxygen species, which in turn depend on the type of support, loading and dispersion of active metals[37].

In this paper, we prepared a series of mesoporous nanostructured $VO_x/Ce_xZr_{1-x}O_2$ catalysts through a surfactant-assisted method for the ODHP and DHP. The structural and textural properties of the prepared $VO_x/Ce_xZr_{1-x}O_2$ nano-catalysts were characterized by a combination of thermogravimetric and differential scanning calorimetry (TG-DSC), transmission electron microscopy (TEM), X-ray powder diffraction (XRD), N_2 adsorption-desorption isotherms, ultraviolet and visible spectrophotometry (UV-vis), H_2-temperature-programmed reduction (H_2-TPR), Raman and X-ray photoelectron spectroscopy (XPS) methods. The effects of the VO_x content, calcination temperature and Ce/Zr ratio on the catalytic activity of these mesoporous $VO_x/Ce_xZr_{1-x}O_2$ catalysts were also studied in detail.

2. Experimental

2.1 Catalyst Preparation

The ceria-zirconia mixed oxides $Ce_xZr_{1-x}O_2$ (x = 0, 0.2, 0.5, 0.8, 1) were synthesized utilizing a surfactant-assisted method of nanoparticle assembly. Specifically speaking, 6 mmol of cetyltrimethylammonium bromide (CTAB) was dissolved in 200 mL distilled water under 15 min ultrasound irradiation at room temperature, then a calculated amount of $Ce(NO_3)_2$•$6H_2O$ and a calculated amount of $Zr(NO_3)_4$•$5H_2O$ were added. After vigorously stirring for 0.5 h, NaOH solution (0.2 mol/L) was dropwise added to the above solution until the pH value of the mixed solution became 10. Next, the mixed solution was further stirred vigorously for 12 h. The final suspended solution was aged for 3 h at 90 °C, then washed using hot water, then dried in an oven for 6 h at 110 °C, finally milled and calcined for 2 h at 500 °C.

The supported vanadium-based catalysts were synthesized by a wet impregnation method utilizing an ammonium metavanadate solution. The NH_4VO_3 was dissolved in water by heating slowly, and then, the finely powdered mixed oxide support was added to the clear solution. The excess water was then evaporated, and the resulting solid was dried at 110 °C in air for 6 h, followed by calcination at 600 °C for 6 h. The vanadia loading contents were 2, 4, 8, 10, and 15 wt%, and the corresponding $VO_x/Ce_{0.8}Zr_{0.2}O_2$ catalysts were named as 2VCe8Zr2, 4VCe8Zr2, 8VCe8Zr2, 10VCe8Zr2 and 15VCe8Zr2, respectively. The catalysts with 8 wt% vanadia loading supported on $Ce_xZr_{1-x}O_2$ of different Ce/Zr ratio (CeO_2, $Ce_{0.8}Zr_{0.2}O_2$, $Ce_{0.5}Zr_{0.5}O_2$, $Ce_{0.2}Zr_{0.8}O_2$ and ZrO_2) were denoted as 8VCe, 8VCe8Zr2, 8VCe5Zr5, 8VCe2Zr8 and 8VZr, respectively. The textural and composition properties of the catalysts are presented in **Table 1**.

Table 1. Chemical composition and textural properties of the catalysts

Catalysts	Calcination temperature (°C)	Mean particle size (nm)	Surface area[a] (m^2/g)	Pore volume[b] (cm^3/g)	$D_{BJH\text{-}ad}$[c] (nm)	$D_{BJH\text{-}de}$[d] (nm)	Average pore diameter$_e$ (nm)
CeO_2	500	8.3	139	0.161	2.7	4.5	4.6
$Ce_{0.8}Zr_{0.2}O_2$	500	6.2	106	0.109	3.3	3.6	4.1
$Ce_{0.5}Zr_{0.5}O_2$	500	4.4	102	0.106	3.2	3.5	3.8
$Ce_{0.2}Zr_{0.8}O_2$	500	7.3	169	0.180	3.6	3.6	4.2
ZrO_2	500	6.1	146	0.156	2.6	3.5	4.3

Table 1. Chemical composition and textural properties of the catalysts Continuation Table:

Catalysts	Calcination temperature (°C)	Mean particle size (nm)	Surface area[a] (m^2/g)	Pore volume[b] (cm^3/g)	$D_{BJH\text{-}ad}$[c] (nm)	$D_{BJH\text{-}de}$[d] (nm)	Average pore diameter[e] (nm)
2VCe8Zr2	500	6.2	106	0.130	2.9	4.0	4.9
4VCe8Zr2	500	6.2	99	0.104	4.0	3.6	4.2
8VCe8Zr2	500	6.2	92	0.085	3.4	3.6	3.7
10VCe8Zr2	500	6.2	84	0.098	5.1	3.6	4.6
15VCe8Zr2	500	6.2	68	0.092	4.9	3.6	5.4
8VCe	500	8.3	61	0.122	7.4	5.8	7.9
8VCe5Zr5	500	4.4	80	0.085	3.4	3.5	3.6
8VCe2Zr8	500	7.3	148	0.159	3.9	4.5	4.3
8VZr	500	6.1	146	0.160	3.4	3.5	4.4
8VCe2Zr8	550	7.6	101	0.138	5.2	4.1	5.5
8VCe2Zr8	600	8.3	44	0.122	1.2	0.7	1.1
8VCe2Zr8	650	10.4	22	0.093	2.7	1.3	1.7
8VCe2Zr8	700	12.1	16	0.098	3.5	1.8	2.5

[a]: Multipoint BET surface area; [b]: Total pore volume at $P/P_0 = 0.99$; [c]: Maximum of the BJH pore diameter as determined from the adsorption branch; [d]: Maximum of the BJH pore diameter as determined from the desorption branch; [e]: BJH average pore diameter (4V/A)

2.2 Catalyst Characterization

The XRD were operated on a Rigaku D/max-2500 diffractometer with Cu K_α radiation at 40 kV and 100 mA. The TEM was performed on a FEI Tecnai G20 microscope. The trace content of samples were ultrasonic dispersed in ethanol solution for 10 min, and then deposited on carbon coated copper grid as TEM samples. The TG-DSC measurements were carried out making using of a TA SDT Q600 instrument using referential α-Al_2O_3 under N2 atmosphere at a heating rate of 5 °C/min. N_2 adsorption-desorption isotherms were carried out on a Quantachrome NOVA 2000e sorption analyzer at liquid nitrogen temperature (77 K). Before measured, the samples were degassed at 200 °C overnight. The surface area and pore size distribution of the samples were calculated by the Brunauer-Emmett-Teller (BET) method and the Barret-Joyner-Halenda (BJH) model, respectively. Temperature-programmed reduction (TPR) was performed over 50 mg of a catalyst at a heating rate of 10 °C/min under a mixture of 5% H_2 in a N_2 flow (30 mL/min). A thermal conductivity detector (TCD) was used to measure the uptake amount during the reduction process. The Raman spectroscopy measurement was carried out on a LabRAM HR800 spectrometer (Horiba Jobin Yvon, France) with a charge-coupled device (CCD) detector at ambient temperature and a 514 nm single-frequency laser under moisture-free conditions. For the purpose of avoiding the thermal damage during operation, the sample was mounted in a spinning holder. The XPS was conducted on a Perkin-Elmer PHI 5600 spectrophotometer with MgK_α radiation. The operating conditions remained unchanged at 187.5 eV and 250.0 W. The C1s peak was fixed at a binding energy of 284.6 eV in order to subtract the surface charging effect. Diffuse reflectance UV-vis absorption spectroscopy was conducted on a JASCO V-570 UV-V-NIR spectrophotometer with barium sulphate as the reference.

2.3 Catalytic Testing

The ODHP and DHP reactions were performed in a fixed bed quartz reactor (Φ = 8 mm) containing 0.5 g catalyst at atmospheric pressure. Mixed gases consisting of 10% O_2, 10% C_3H_8 and 80% N_2 with a total flow rate of 50 mL/min, and 90% N_2 and 10% C3H8 with a total flow rate of 50 mL/min, were utilized as the reaction gases for the ODHP and DHP reactions, respectively. The reaction temperatures ranging from 200 °C to 600 °C at 50 °C intervals were performed. The reaction products were detected by online chromatographic analysis with a TCD detector using a TDX-01 column for O_2, CO, CO_2 and CH_4 separation, an OV-1 column for C_3H_8, C_3H_6, C_2H_4, CH_4 and H_2 separation, and He as a carrier gas.

3. Results and discussion

3.1 Characterization of the Catalysts

3.1.1 Thermogravimetric analysis

The TG-DSC result of the $Ce_xZr_{1-x}O_2$ precursor is revealed, as shown in **Figure 1**. It can be obviously observed that the endothermic peak between 75 °C and 180 °C on the DSC pattern, coupled with an arresting weight loss on the TG curve, can be attributed to the desorption of the chemical and/or physical adsorbed water located on the catalyst surface and/or pore structure of the catalyst. The dominating weight loss on the TG curve between 180 °C and 480 °C, along with a strong exothermic peak at 220 °C and a shoulder at approximate 255 °C, belongs to the pyrolysis of the carbon species and the decomposition of the surfactant. It is also found that the total weight loss is 18.8 wt%. Besides, no obvious crystalline phase transformation can be observed. After the temperature rises to 500 °C, the weight of the precursor no longer changes, indicating that the carbon species (surfactant molecules) in the catalyst can be eliminated completely after calcination in air at 500 °C. Thus, for the studied vanadia-based catalysts, the proper calcination temperature under air atmosphere is 500 °C because the extortionate temperature calcination can lead to an increase of catalyst size and a reduction of specific surface area.

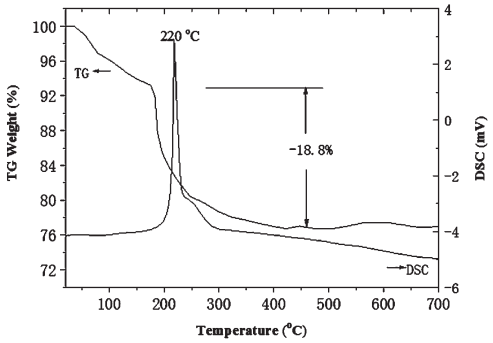

Figure 1. TG/DSC patterns of the precursor of $Ce_xZr_{1-x}O_2$

3.1.2 X-ray diffraction

The XRD patterns of the synthesized $VO_x/Ce_{0.8}Zr_{0.2}O_2$ catalysts with different content of vanadia loading are presented in **Figure 2a**. The main reflections are at 28.6°, 33.3°, 47.5° and 56.8° (2θ) corresponding to the cubic fluorite structure of CeO_2. Besides, no obvious other phases are detected. This indicates that the ZrO_2 dopant is contained within the lattice of CeO_2, maintaining the fluorite structure while forming a solid solution[32]. As shown in **Figure 2a**, when the vanadia content is below 10 wt%, no XRD reflections of V_2O_5 and $CeVO_4$ structure are present, which indicates that the supported vanadia species are highly dispersive on the support surface and the size of powdery particles are too tiny to be detected by the conventional XRD method. However, when the vanadia content rises to 15 wt%, the weak diffraction peaks appeared at 24.0° and 32.7° (2θ) are attributed to the CeVO4 crystal phase. Daniell and coworkers suggested that CeO_2 and VO_x species would react to form $CeVO_4$ at 573 K[35].

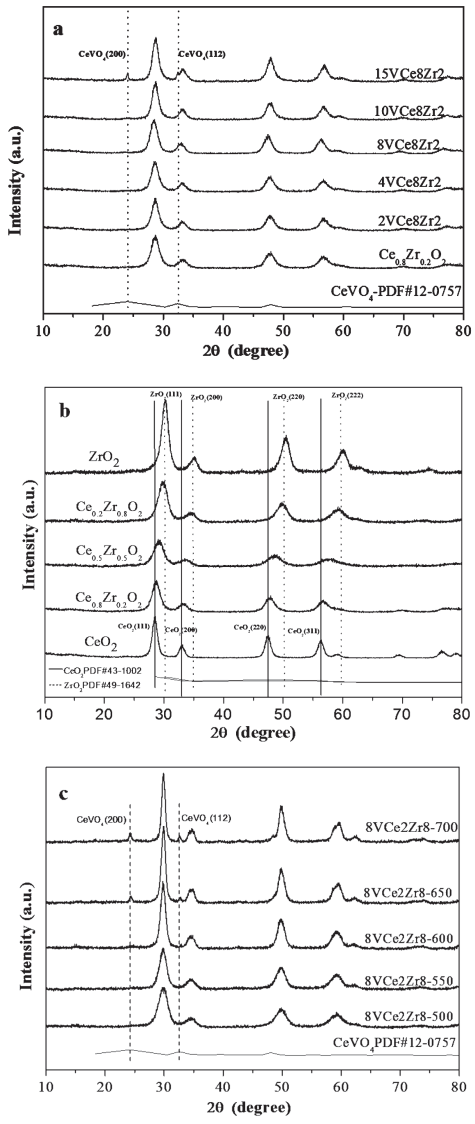

Figure 2. (a) XRD patterns of the catalysts with different VO_x contents supported on $Ce_{0.8}Zr_{0.2}O_2$ calcined at 500 °C; (b) XRD patterns of $Ce_xZr_{1-x}O_2$ mixed oxides calcined at 500 °C; (c) XRD patterns of catalyst 8VCe2Zr8 calcined at different temperatures

The XRD spectra of the mixed Ce-Zr oxide supports are shown in **Figure 2b**. As the Ce content varies, the support Ce-Zr oxides exhibit a phase transition from cubic structure to tetragonal structure where the ideal fluorite-type structure has the space group *Fm*-3*m* while the tetragonal phase belonging to the $P4_2/nmc$ group has oxygen displacements from an ideal fluorite position[38]. This suggests the formation of Ce-Zr-O solid solutions. It is previously indicated that the $Ce_xZr_{1-x}O_2$ solid solutions have a tetragonal structure when $x \leqslant 0.5$ and a fluorite-type cubic structure when $x > 0.5$[39]. From **Figure 2a**, the ceria and $Ce_{0.8}Zr_{0.2}O_2$ are crystallized in a cubic fluorite-type structure. The main diffraction peaks located at $2\theta \approx 28.6°$ and 47.5° are shifted towards higher diffraction angles for the cerianite structure, after the introduction of ZrO_2 in the CeO_2 lattice. This was attributed to the shrinkage of the lattices on account of the replacement of Ce^{4+} with a smaller Zr^{4+}, being in agreement with the Vegard rule[40]. The tetragonal structure typical of CeO_2 appeared with $x > 0.5$.

The XRD patterns of a series of 8VCe2Zr8 catalysts calcined at different temperatures are shown in **Figure 2c**. With an increase in the precalcination temperature of the 8VCe2Zr8 catalysts from 500 °C to 700 °C, the relative strength of $Ce_{0.2}Zr_{0.8}O_2$ phase increases gradually, indicating that the crystallinity and the particle size of support $Ce_{0.2}Zr_{0.8}O_2$ increase after high-temperature heating treatment. When the catalyst was calcined at 650 °C and above, two weak diffraction features of $CeVO_4$ structure at 24.0° and 32.7° (2θ) were observed, indicating that the reaction of VO_x and CeO_2 occurred after high temperature calcination. The V coverage also results in the formation of $CeVO_4$, originating from the intimate contact between the $Ce_{0.2}Zr_{0.8}O_2$ support and the dispersed VOx species, which indicates that the formation of $CeVO_4$ is more easily than ZrV_2O_7. The mean particle sizes of $Ce_{0.2}Zr_{0.8}O_2$, calculated by the Scherrer's equation with a half width of the diffraction peak of the (111) plane, are presented in **Table 1**. It is seen that the mean particle sizes of the $Ce_{0.2}Zr_{0.8}O_2$ are in the range of 7.3-12.1 nm when the calcination temperature of catalysts was from 500 to 700 °C.

3.1.3 Nitrogen adsorption-desorption analysis

The nitrogen adsorption-desorption isotherms and the corresponding pore size distributions of the $Ce_xZr_{1-x}O_2$ supports and the $VO_x/Ce_xZr_{1-x}O_2$ catalysts with different vanadia contents and calcined at different temperatures are shown in **Figures 3-5**, and the- textual properties are listed in **Table 1**. The isotherms of all the surfactant-assisted synthesized catalysts exhibit a classical type IV which is the symbol of typical mesoporous materials. At a high relative pressure (P/P_0) range, a well-defined hysteresis loop, coupled with a relatively sharp steep desorption branch and a sloping adsorption branch is observed, indicating that the effective radii of the narrow entrances are of equal size while the effective radii of the mesopores are heterogeneously distributed[41]. The H2-type of the hysteresis loop is typical for hierarchical scaffold-like mesoporous structures and wormhole-like mesostructures deriving from the surfactant-assisted nanoparticle assembly[41,42].

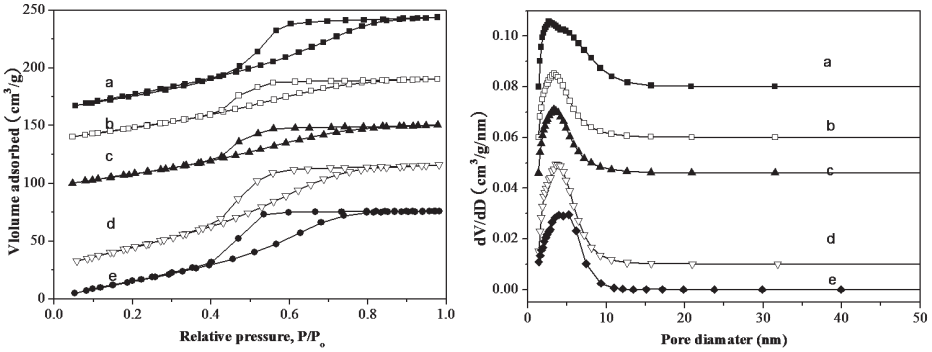

Figure 3. (*left)* N_2 sorption-desorption isotherms and (*right*) the corresponding pore size distribution curves of the $CexZr_{1-x}O_2$ support with different Ce/Zr ratios: (a) CeO_2, (b) $Ce_{0.8}Zr_{0.2}O_2$, (c) $Ce_{0.5}Zr_{0.5}O_2$, (d) $Ce_{0.2}Zr_{0.8}O_2$, (e) ZrO_2. The volume was shifted by 140, 120, 90, 0 and -25 for the curves of datasets a-e, and the dV/dD value was shifted by 0.08, 0.06, 0.04 and 0.01 for the curves of datasets a-e, respectively

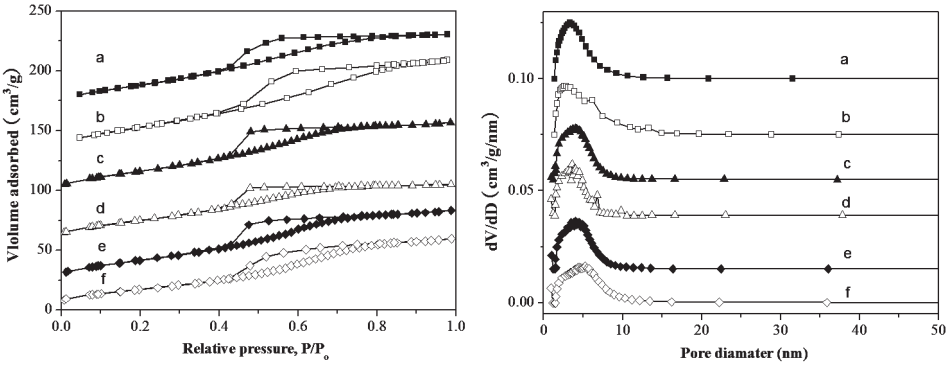

Figure 4. (*left*) N_2 sorption-desorption isotherms and (*right*) the corresponding pore size distribution curves of the VO_x/$Ce_{0.8}Zr_{0.2}O_2$ catalysts with different VO_x contents: (a) $Ce_{0.8}Zr_{0.2}O_2$, (b) 2VCe8Zr2, (c) 4VCe8Zr2, (d) 8VCe8Zr2, (e) 10VCe8Zr2, and (f) 15VCe8Zr2. The volume was shifted by 160, 125, 90, 50 and 20 for the curves of datasets a-e, and the dV/dD value was shifted by 0.1, 0.075, 0.055, 0.04 and 0.015 for the curves of data sets a-e, respectively

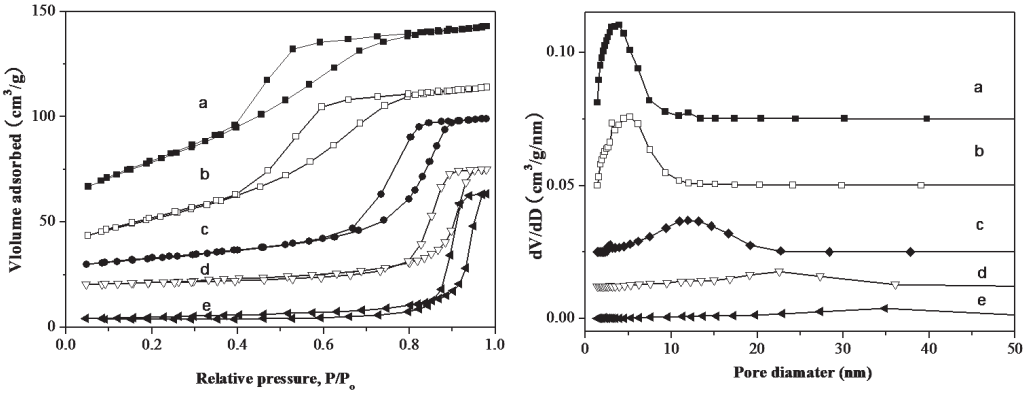

Figure 5. (*left*) N_2 sorption-desorption isotherms and (*right*) the corresponding pore size distribution curves of the 8VCe2Zr8 catalysts calcined at different temperatures: (a) 500 °C (b) 550 °C, (c) 600 °C, (d) 650 °C, and (e) 700 °C. The volume was shifted by 40, 25, 20 and 15 for the curves of the datasets a-d, and the dV/dD value was shifted by 0.075, 0.05, 0.025 and 0.012 for the curves of datasets a-d, respectively

The N_2 adsorption isotherms of the prepared catalysts present an obvious increase in the P/P_0 range of 0.2-0.4, which is typical characteristic of capillary condensation within mesopores. The pore size distribution curves of the $Ce_xZr_{1-x}O_2$ supports and the VO_x/$CexZr_{1-x}O_2$ catalysts with different vanadia contents present one single peak centered at 2.6-3.6 and 2.9-5.1 nm (**Figures 3 and 4**), respectively, manifesting the porosity is homogeneous. As the vanadia content increases from 0 to 15 wt%, the surface area of the catalyst decrease from 106 to 68 m^2/g (**Table 1**), mainly due to the agglomeration of vanadia species on the $Ce_{0.8}Zr_{0.2}O_2$ support. The pore size distributions of the 8VCe2Zr8 catalysts calcined at different temperatures are also narrow while the pore size increases with the calcination temperature (**Figure 5**). The average pore diameters of the 8VCe2Zr8 catalysts increase from 4.4 to 5.5 nm when the calcination temperature is from 500 to 550 °C, while the surface areas decrease from 148 to 101 m^2/g (**Table 1**). With a calcination temperature at 700 °C, the location of the inflection point in the isotherms of 8VCe2Zr8 moved to a higher P/P_0 range of 0.7-0.9, indicating an increase in the pore size, while the surface areas decreased to 16 m^2/g (**Table 1**). According to **Table 1**, the vanadia addition can significantly affect the textural properties of the resultant catalysts. The surface area of the high Ce content support ($Ce_{0.8}Zr_{0.2}O_2$) and the CeO_2 support shrinks to a great certain due to the addition of V, indicating that the V species tend to block the pore structure of CeO_2 corresponding to the obvious reduction of the pore volume after the V introduction. With the V addition to high Zr content support ($Ce_{0.2}Zr_{0.8}O_2$) and pure ZrO_2 support, the reduction of those supports become unobvious. The

high Zr content of $Ce_xZr_{1-x}O_2$ supports may help the distribution of VO_x species and inhibit the formation of large VO_x agglomeration.

3.1.4 Transmission electron microscopy

The TEM images of the $Ce_{0.8}Zr_{0.2}O_2$ and 8VCe8Zr2 samples calcined at 500 °C are presented in **Figure 6**. It is clearly indicated that the $VO_x/Ce_{0.8}Zr_{0.2}O_2$ catalysts with different vanadia loading content possess wormhole-like disordered mesoporous structures resulting from the agglomeration of the uniform nanoparticles. The accessible pores are connected randomly, lacking a discernible long-range order among the small $Ce_{0.8}Zr_{0.2}O_2$ particles, which is well in agreement with the N_2 adsorption–desorption isotherms. The nanoparticles in these prepared catalysts demonstrate regular shapes with particle sizes of approximately 4 nm, consistent with the crystallite size calculated from the XRD patterns.

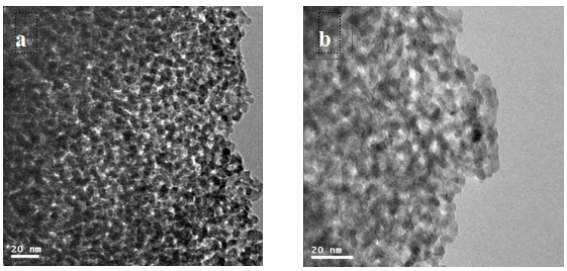

Figure 6. TEM images of (a) $Ce_{0.8}Zr_{0.2}O_2$ and (b) 8VCe8Zr2 catalysts calcined at 500 °C

3.1.5 Temperature-programmed reduction with hydrogen

It is believed that the oxidative dehydrogenation reactions of alkanes over supported transition metal oxides are carried out by a redox mechanism, and the reductive ability of the catalyst plays an important role. Thus, the reduction properties of the mixed oxide supports were studied by temperature-programmed reduction; the hydrogen consumption profiles as a function of temperature are plotted in **Figure 7**. CeO_2 is well known to undergo surface and bulk reductions at approximately 520 °C and 800 °C, respectively. The former peak at 520 °C is well corresponding to the reduction peak of the Ce^{4+} species on catalyst surface, which is depending a lot to the surface area of the support. The latter originates from the bulk reduction of the oxide[41]. The TPR curve of the $Ce_{0.8}Zr_{0.2}O_2$ support presents a primary reduction peak at approximately 520 °C and another weak and broad reduction peak at about 780 °C (**Figure 7a**). The low-temperature peak at 520 °C is more dominant compared to the TPR profile of CeO_2. These results are consistent with the findings of previous studies of $Ce_xZr_{1-x}O_2$[43,44], indicating that the introduction of Zr element into CeO_2 increased the reducibility of Ce^{4+} species because of the increase of the oxygen mobility for oxides with intermediate Ce/Zr ratios. Pure V_2O_5 can be reduced in four characteristic steps at H_2 atmosphere. As reported by Machold *et al.*[45], the four-step reduction process of V_2O_5 could be depicted as: $V_2O_5 \rightarrow V_6O_{13} \rightarrow VO_2 \rightarrow VnO_2n-1 \rightarrow V_2O_3$ ($4 < n < 8$).

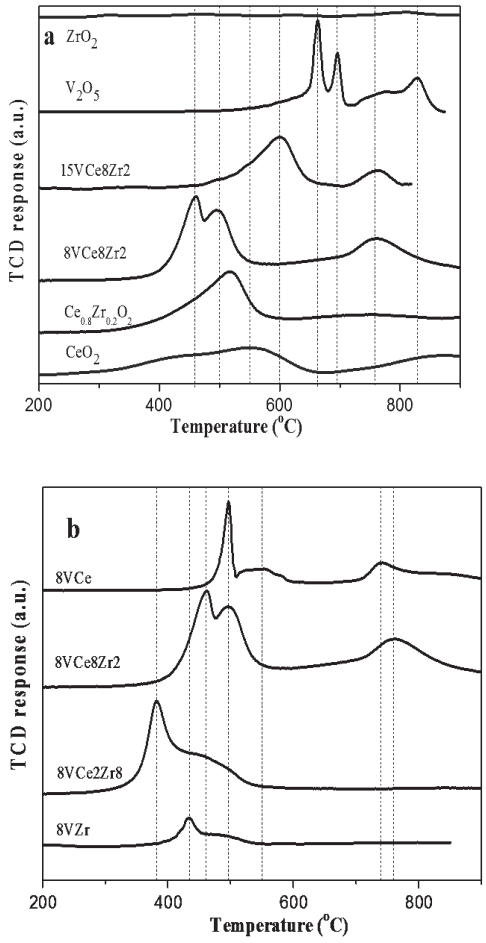

Figure 7. H_2-TPR profiles of the catalysts

The TPR curves of the $VO_x/Ce_xZr_{1-x}O_2$ catalysts present peaks which are generally shifted to lower temperatures compared to pure V_2O_5 bulks. For 8VCe2Zr8, new reduction peak appeared with a maxima at 460 °C and the broader peak becomes visible (780 °C).

The first reduction peak is derived from the formation of polymeric and monomeric VO_x species on the $Ce_xZr_{1-x}O_2$ support surface and the interaction between the VOx species and the $Ce_xZr_{1-x}O_2$ support[45]. An increase of vanadia loading to 15% results in more altering in the TPR profile, namely, the peak at 520 °C assigned to the surface CeO_2 species disappeared, and two reduction peaks can be observed at 620 and 780 °C. Ten percent V_2O_5 is close to the monolayer capacity, suggesting that the coating VOx species on the $Ce_xZr_{1-x}O_2$ surface inhibited the reduction of Ce^{4+} species located in the bulk and on the catalyst surface. In agreement with the literature[46,47], it is indicated that the catalysts containing V_2O_5 are more difficult to be reduced compared to the samples with vanadate species, which is identical to the decreased degree of V dispersion. Obviously, the peaks at above 500 °C can serve as an indicator of the existence of agglomerated V_2O_5 phase. However, the reduction temperature of the pure V_2O_5 is still higher than that of V_2O_5-containing catalysts. The peak at 780 °C corresponded to reduction of $CeVO_4$[48]. This result is consistent with the XRD results.

The reductive ability of the VO_x species interacting with different supports has already been investigated[24,25,49]. It is revealed that the small polymeric species are reduced more rapid at lower temperatures than the large polymeric species and isolated structures. **Figure 7b** shows the TPR curves of the catalysts with 8 wt% vanadia supported on $Ce_xZr_{1-x}O_2$. The reduction peaks of catalyst 8VCe appear at 500, ~550 and ~780 °C. The low temperature peaks (500~600 °C) are attributed to a combination of two redox couples: V^{5+}/V^{4+} and Ce^{4+}/Ce^{3+}. The high-temperature peak is attributed to Ce^{4+}/Ce^{3+} in the bulk. With a decreasing cerium content, the low-temperature peaks (500~600 °C) shift to a lower temperature, whereas the higher temperature peak gradually disappeared. Clearly, this phenomenon implied that the formation of $Ce_xZr_{1-x}O_2$ solid solution through introducing ZrO_2 into the CeO_2 lattice promoted the release of the bulk lattice oxygen while the different Ce/Zr ratios of the supports influenced the formation of VO_x species on the $Ce_xZr_{1-x}O_2$ surface.

3.1.6 Raman spectroscopy

Raman spectroscopy was utilized to measure the structure of the VO_x species both in crystalline and amorphous form. The Raman spectrum (**Figure 8**) of 8VCe8Zr2 shows smaller bands at 239 and 590 cm^{-1} and a large band at 460 cm^{-1}. These Raman bands are the most intense ones for CeO_2[36]. The intensity of the band at 460 cm^{-1} nearly disappears in 8VCe2Zr8. For 8VCe2Zr8 catalyst, new Raman spectrum bands appear at 310 and 630 cm^{-1}, which are typical characteristics of the monoclinic phase of ZrO_2[43]. These findings corroborate the XRD data. The band at approximately 1010 cm^{-1} in 8VCe8Zr2 and 8VCe2Zr8 is corresponding to the isolated species (V = O stretching mode). However, the coexistence of the broad at approximately 837 cm^{-1} indicates the V–O–V modes in the polyvanadate structures[49]. Martínez-Huerta *et al*.[36] observed that $CeVO_4$ exhibited an intense Raman band at 755 and 839 cm^{-1}. Thus, the attribution of the band at 750 cm^{-1} in the spectra of 8VCe8Zr2 to the Ce-O-V stretching mode is reasonable, indicating that the surface vanadium species interact with the $Ce_xZr_{1-x}O_2$ supports.

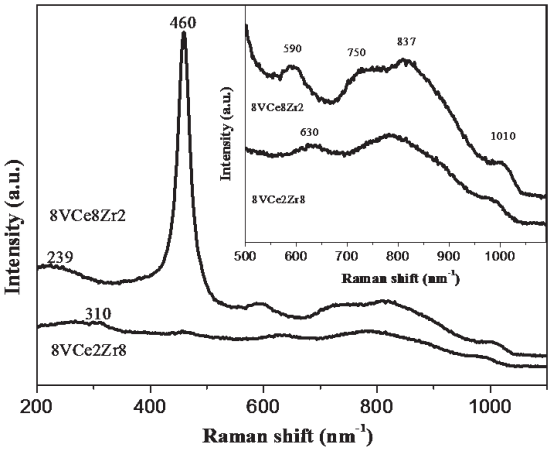

Figure 8. Raman spectra of the 8VCe8Zr2 and 8VCe2Zr8 catalysts

3.1.7 Diffuse reflectance UV-vis spectroscopy

Figure 9 illustrates a comparison of the diffuse reflectance spectra of 8VCe8Zr2 and 8VCe2Zr8 catalysts. These spectra exhibit charge-transfer bands below 500 nm. The CT bands at 320 nm and 244 nm can be assigned to the tetrahedral chains of VO_x linked to each other by V-O-V bridges and isolated tetrahedral VO_x[50]. An additional weak band at 340 nm is observed in these catalysts, revealing the presence of either isolated octahedrally coordinated or oligomeric tetrahedrally V5+ species[50]. The bands centered at ca. 243-250 and 315-320 nm assigned to the O→V bonds are also well conformed to the reported VO_x catalysts on different supports[16,17,51,52]. The band at highly aggregated vanadia entities, related to the 484 nm[50], cannot be observed in the spectra, indicating no aggregated VO_x species arise on the 8VCe8Zr2 and 8VCe2Zr8 catalysts. The results are well corresponding to the XRD, H_2-TPR and Raman results, which suggest the vanadia species are finely dispersed on the catalyst surface. However, the absorption edge energies of these two catalysts are different. The energy decreases with the increase of the Ce/Zr ratio of the supports, reflecting an increase in the dimensionality and size of the VO_x domains with the vanadium surface density increases[52]. Below the vanadium surface density, the ratio of isolated/polymeric surface vanadium species decreases continuously with the vanadium surface density. The percentage of vanadium species on the polymeric surface with bridging V-O-V bonds in the vanadium phase of the dehydrated supported can also be quantified from the UV-vis DRS edge energy (E_g) values in the sub-monolayer region[53]. Thus, the polymeric surface vanadium species of 8VCe2Zr8 are greater than those of 8VCe8Zr2. This may be one of the reasons that the low-temperature reduction peaks (500~600 °C) shift to a lower temperature with a decrease in the cerium content during temperature-programmed reduction with hydrogen. However, the isolated species are more different to be reduced than the aggregated surface VO_4 species[10,24].

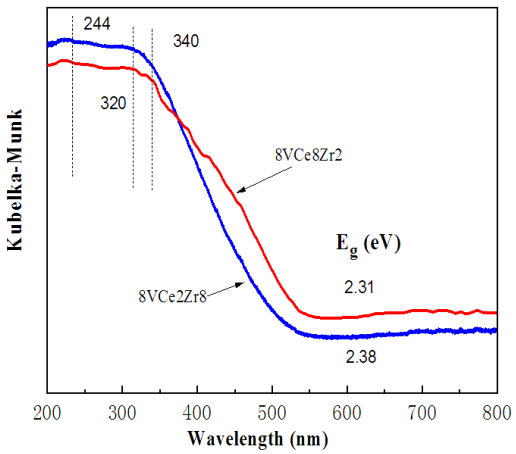

Figure 9. Diffuse reflectance UV-vis spectra of the 8VCe8Zr2 and 8VCe2Zr8 catalysts

3.1.8 X-ray photoelectron spectroscopy

For the purpose of acquiring explicit information on the chemical states of the anions and cations and determining the surface composition of the prepared catalysts, X-ray photoelectron spectroscopy was conducted. The XPS V 2p spectra of 8VCe8Zr2 and 8VCe2Zr8 are shown in **Figure 10a**. The V valence states were determined taking the V $2p_{3/2}$ peak into account. After Shirley background subtraction, the V $2p_{3/2}$ peaks were fitted with Gaussian-Lorentzian curves, and the results are reported in **Table 2**. The V^{3+}, V^{4+} and V^{5+} oxidation states were asserted when the binding energies of V $2p_{3/2}$ were 514.0 eV, 516.2 eV and 517.1 eV, respectively. In the fresh catalysts 8VCe8Zr2 and 8VCe2Zr8, V^{5+} and V^{4+} could be detected[18,45], but V^{3+} was not identified. However, the surface V^{5+}/V^{4+} ratio is different. For 8VCe8Zr2, V^{5+} is the main vanadium state. Because of the increase in the V^{4+} content, the 8VCe2Zr8 catalyst shows initial oxidation states of ~4.5, indicating that the "polyvanadate" net structure reported by Klose[54] comprises the chains with $[V_3O_7]^-$ as the base unit on the surface.

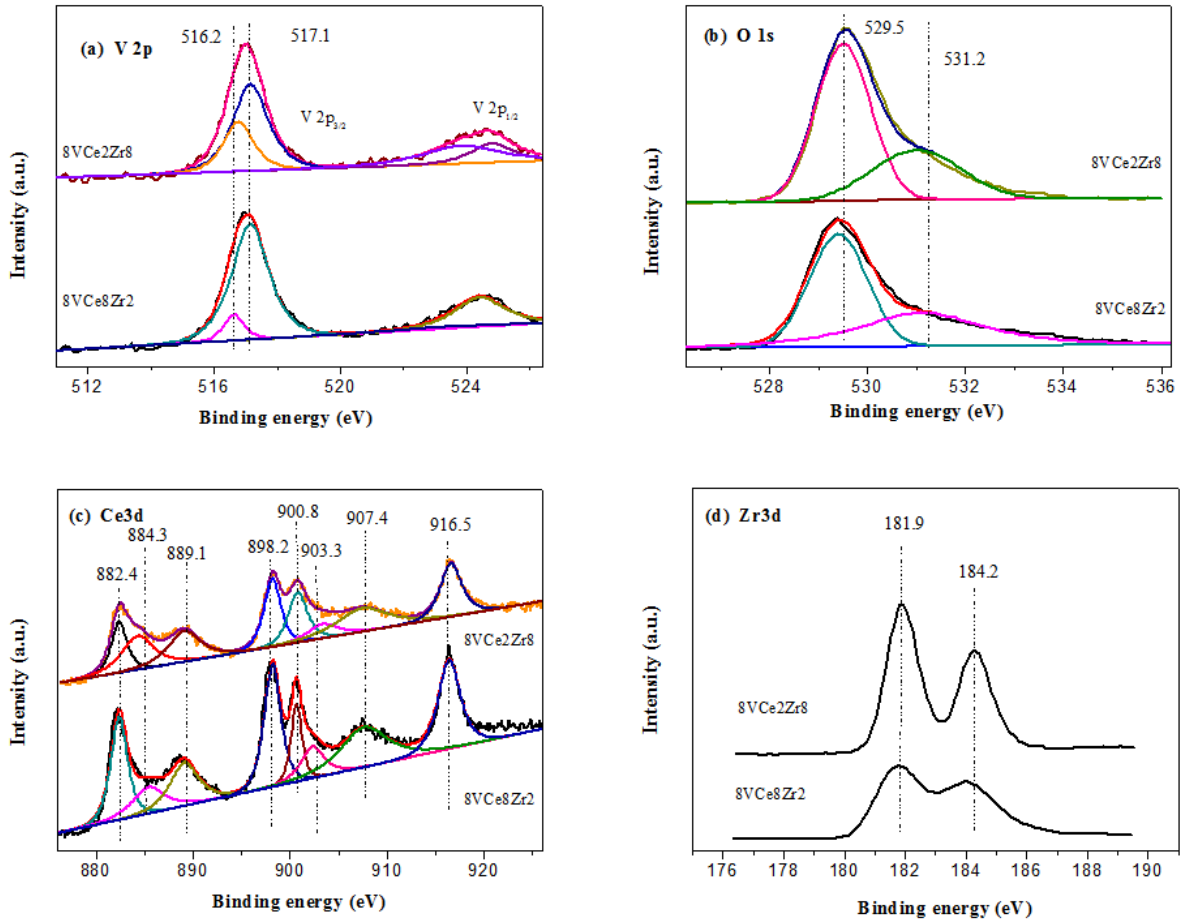

Figure 10. XPS analysis of the 8VCe8Zr2 and 8VCe2Zr8 catalysts: (a) V 2p spectrum; (b) O 1s spectrum; (c) Ce 3d spectrum; and (d) Zr 3d spectrum

Table 2. Surface V^{4+}/V^{5+}, Ce^{3+}/Ce^{4+} and Ce/Zr ratios of the catalysts estimated according to the XPS results

Catalyst	Surface V^{4+}/V^{5+} ratio	Surface Ce^{3+}/Ce^{4+} ratio	Surface Ce/Zr ratio
8VCe8Zr2	0.13	0.12	4.88
8VCe2Zr8	0.48	0.13	0.31

As depicted in **Figure 10b**, the O 1s peak at BE = ca. 529.4 eV can be deconvoluted into two components: one at 531.6 eV and the other at 529.5 eV. The former is attributable to surface hydroxyl group species, while the latter is attributable to surface lattice oxygen[38].

In **Figure 10c**, two sets of Ce 3d signals are evident: one set has peaks at BE = 900.8, 903.3, 907.4 and 916.5 eV attributing to Ce $3d_{3/2}$, while the other set has peaks at BE = 882.4, 884.3, 889.1 and 898.2 eV attributable to Ce $3d_{5/2}$[38,55]. The signals at BE = 884.3 and 903.3 eV are corresponding to Ce^{3+}, while the others are corresponding to Ce^{4+}[38,55]. The coexistence of Ce^{4+} and Ce^{3+} ions indicate the presence of oxygen vacancies in/on the catalysts. The V^{5+}-O^{2-}-Ce^{3+} sites result from the well-dispersed vanadia on the CeO_2 support[36]. A reduction in the values of the BE of the Ce $3d_{5/2}$ (882.4 eV) appears compared to that of bulk CeO_2 (882.9 eV). This shift can be explained by the established interaction between the ZrO_2 and CeO_2, i.e., the formation of Ce–O–Zr bonds[38].

Figure 10d manifests the photoemission spectra of Zr 3d of the prepared catalysts which exhibit a doublet corresponding to Zr $3d_{5/2}$ approximately 181.9 eV and Zr $3d_{3/2}$ approximately 184.2 eV. Interestingly the binding energy of Zr $3d_{5/2}$ is lower than that in ZrO_2 (182.9 eV), but higher than that in Zr metal (180.0 eV), and similar to ZrO_x ($0 < x < 2$, 181.4 eV)[38]. Thus, the formation of $Ce_xZr_{1-x}O_2$ solid solutions is proved.

The surface atomic contents of V, Ce and Zr are 4.43%, 6.44% and 20.83% for 8VCe2Zr8, and 4.68%, 27.88% and 4.35% for 8VCe8Zr2, respectively, estimated by XPS. For 8VCe8Zr2 and 8VCe2Zr8,

the surface atomic ratios of V/(V+Ce+Zr) are 0.139 and 0.126, respectively, which are higher than those calculated for the preparation. Consequently, the isolated and polymeric VO_x species spreading on the surface of catalysts are deriving from the vanadium oxides[45]. With regard to the Ce/Zr atomic ratio, it should be noted that the Ce/Zr ratio (4.88 and 0.31) is higher than the nominal atomic ratio (4 and 0.25), indicating surface enrichment in cerium.

3.2 Catalytic Performance

3.2.1 Oxidative dehydrogenation of propane

The catalytic behavior of the synthesized VO_x-based catalysts in the ODHP reaction was studied using a molar ratio of C_3H_8/O_2 at 1:1 as cofeeding gas under a range of reaction temperatures between 200 and 600 °C. With the exception of the ideal product (propylene), the presence of O_2 in the reacting mixture facilitates the oxidation reactions of propane and/or propylene to form CO and CO_2. Small amounts of ethane, ethylene, and oxygenates (e.g. acetaldehyde and acetic acid) were also traced. The values of propane conversion as a function of reaction temperature are shown in **Figure 11**. It is revealed that an increase in the propane conversion with temperature is usually accompanied by an increase of the selectivity toward the carbon oxides and a decrease of the selectivity toward propylene. The catalytic activity of $VO_x/Ce_{0.8}Zr_{0.2}O_2$ catalysts is improved with the increase of VO_x loading content from 2 to 8 wt%, and thus, the 8VCe8Zr2 catalyst demonstrates the highest catalytic activity. However, a further increase in the VO_x content resulted in a decrease in the catalytic activity. The initial activity with the increase of vanadium content may be related to an increase in the concentration of the surface vanadium oxide species. The lower activity of 15VCe8Zr2 must be ascribed to the formation of $CeVO_4$ ($CeVO_4$ has low catalytic activity) due to high vanadium loading[35]. This finding reveals that the activity of the prepared catalysts significantly depend on the dispersion of the surface VO_x species, supported by the XRD and H_2-TPR results. In **Table 1**, the surface area of $VO_x/Ce_{0.8}Zr_{0.2}O_2$ with different VO_x content catalysts initially decreases with vanadia loading and then remains relatively constant, as reported with similar observations[17,35,52,54]. The initial reduction of the surface area might result from the plugging of pore structures. This behavior suggests that 8VCe8Zr2 has the largest amount of monolayer dispersive VO_x species on the surface and the most active species with a higher ODHP activity. The V_2O_5 supporting on mesoporous nanostructured $Ce_{0.8}Zr_{0.2}O_2$ significantly improves the catalytic performance of V_2O_5, which could run this reaction at relatively low temperature (250 °C). The higher conversion of 18.42% was obtained for 8VCe8Zr2 at 350 °C. The conversion of propane at the low temperature upper end of performance data has been reported for cerium-supported vanadium catalysts[35,56]. The higher surface area of mesoporous nanostructured catalysts may promote the higher dispersion of oxidation catalyst nanoparticles, thus improving the catalytic performance.

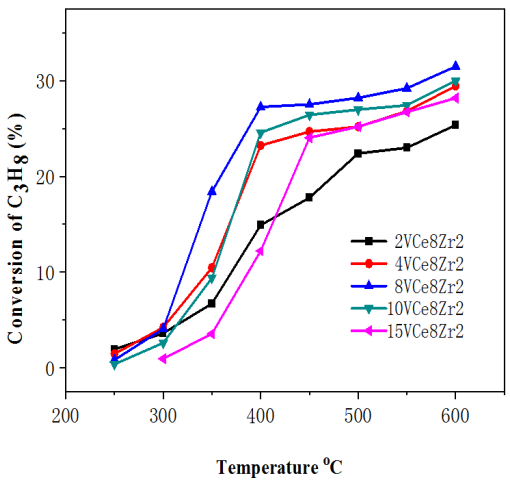

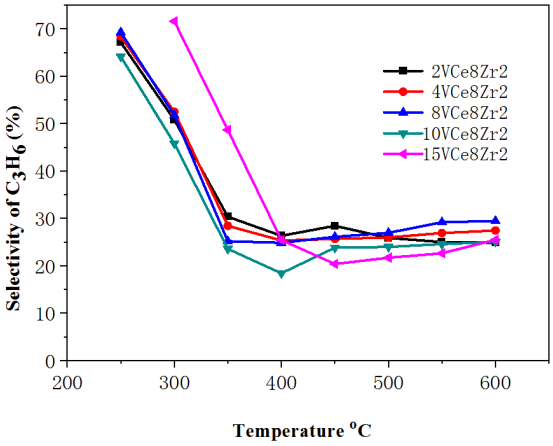

Figure 11. Conversion of C_3H_8 and selectivity to C_3H_6 as a function of the temperature of reaction of the $VO_x/Ce_{0.8}Zr_{0.2}O_2$ catalysts with different VO_x contents

The ODHP activity of the catalysts with 8 wt% VO_x supported on $Ce_xZr_{1-x}O_2$ is presented in **Figure 12**. When compared to the supported pure ceria, the catalysts utilizing binary ceria-zirconia oxides as supports exhibit higher propane conversions. These high conversions may result from the Zr^{4+} ions in the lattice which promote the formation of oxygen vacancies on the surface of the binary oxide supports, determined by the H_2-TPR results. However, this must not be the only reason, as the results of the DR UV-vis, Raman, H_2-TPR and XPS studies indicate that different Ce/Zr ratios of the supports impacted the formation of the VO_x species on the $Ce_xZr_{1-x}O_2$ surface. In addition, the activity of 8VCe2Zr8 is higher than the activity of the 8VZr catalyst, which may be attributed to Ce^{3+} ions appearing on the surface of the binary ceria-zirconia oxide-supported V_2O_5. The coexistence of Ce^{3+} and Ce^{4+} ions suggests the presence of oxygen vacancies on/in the catalysts. The catalytic performance of 8VCe8Zr2 and 8VCe2Zr8 are reported in **Figure 13**. The selectivity toward propylene decreases with the increase of propane conversion, accompanied by increased selectivity toward CO at a lower propane conversion (for 8VCe8Zr2 is < 27% and for 8VCe2Zr8 is < 22%). The selectivity to CO_2 remains rather constant. This behavior indicates that CO is formed from propylene under oxygen-excess conditions. At higher reaction temperatures, the oxygen becomes limiting. The selectivity to CO decreases with the increase of propane conversion, accompanied by an increased selectivity to CO_2. Thus, CO_2 generates at higher propane conversions directly from propane. However, the most interesting results are the increasing selectivity toward propylene with increasing propane conversion under the same conditions. Especially for 8VCe2Zr8, this behavior is obvious. The additional contribution to the formation of propylene may originate from the contributions of the catalytic dehydrogenation and the homogeneous reactions, especially when the reaction process is performed under O_2-lean conditions.

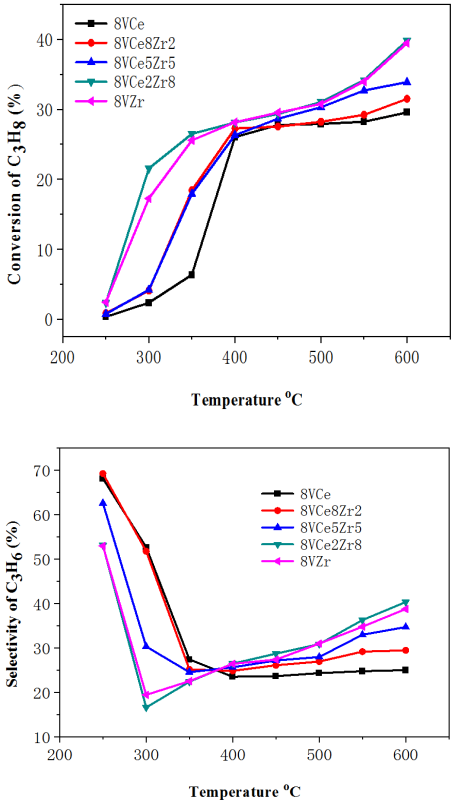

Figure 12. Conversion of C3H8 and selectivity to C_3H_6 as a function of the temperature of reaction of the $8VO_x/Ce_xZr_{1-x}O_2$ catalysts

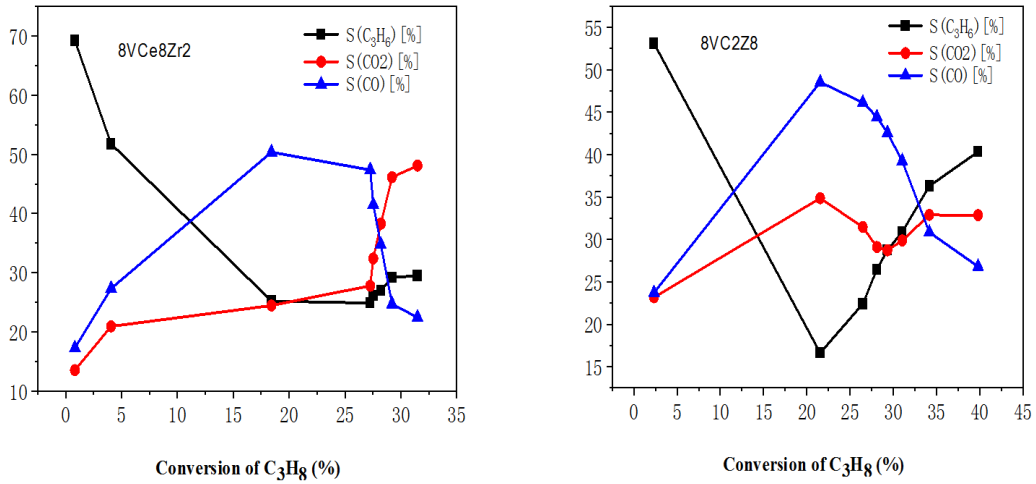

Figure 13. Selectivity to C_3H_6, CO and CO_2 as a function of the degree of the conversion of the C_3H_8 catalytic activity of 8VCe8Zr2 and 8VCe2Zr8 in ODHP

Figure 14 shows the ODHP catalytic performance of the 8VCe2Zr8 catalysts calcined at different temperatures. The catalytic activity of the 8VCe2Zr8 catalyst decreased with the pre-calcination temperature rising from 500 to 700 °C. The loss of activity may be related to the formation of $CeVO_4$ at high calcination temperature. For this series of catalysts, the loss of activity may result from the large decrease of surface area with vanadia loading. In **Figure 14b**, the 8VCe2Zr8 catalyst calcined at 700 °C exhibits a slightly high selectivity to propylene at low reaction temperatures (< 400 °C). Despite its low activity, the better selectivity of the 8VCe2Zr8-700 catalyst must be attributed to the existence of the surface sites with the low reactivity upon the formation of cerium vanadate. The lower selectivity of 8VCe2Zr8-700 at higher reaction temperatures (> 400 °C) may be attributed to the catalytic dehydrogenation of propane to propylene over the surface vanadium species under oxygen limiting conditions, whereas $CeVO_4$ does not demonstrate catalytic dehydrogenation activity.

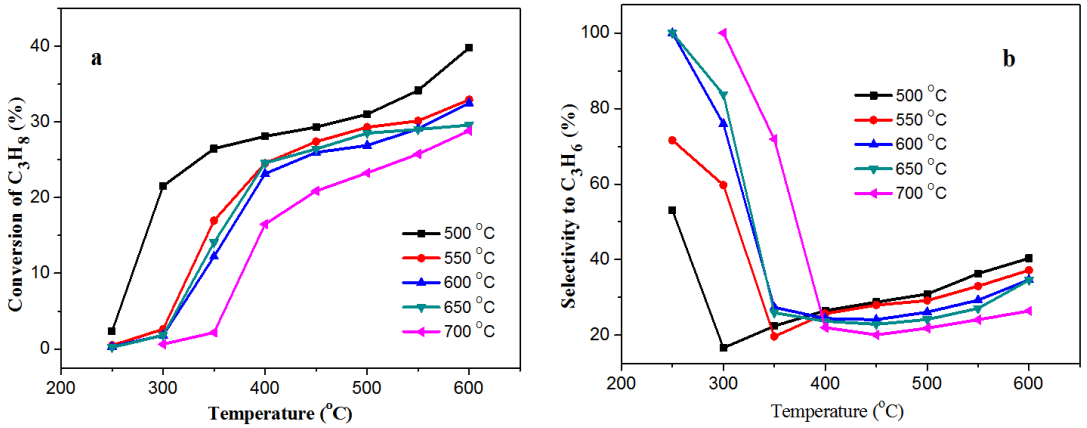

Figure 14. (a) Conversion of C_3H_8 as a function of the temperature of reaction of the 8VCe2Zr8 catalysts calcined at different temperatures; (b) Selectivity to C_3H_6 as a function of the temperature of the reaction of the 8VCe2Zr8 catalysts calcined at different temperatures

3.2.2 Direct dehydrogenation of propane

The activity of 8VCe8Zr2 and 8VCe2Zr8 towards direct propane dehydrogenation was evaluated to study the relationship between the ODHP and catalytic direct dehydrogenation of propane, shown in **Figure 15**. Interestingly, the 8VCe8Zr2 catalyst exhibits less activity for propane conversion and more selectivity for propylene than 8VCe2Zr8 under oxygen-excess

conditions (at a lower reaction temperature). The catalytic dehydrogenation cannot be operated at this temperature. However, the propylene is primarily formed through the direct dehydrogenation of propane instead of the oxidative dehydrogenation pathway with a further increase of the reaction temperature. It can be seen that propane begins direct dehydrogenation to propylene over 8VCe8Zr2 and 8VCe2Zr8 at 350 and 400 °C, respectively. This behavior leads to the increasing selectivity toward propylene with the increasing conversion of propane under oxygen-lean conditions (at a higher reaction temperature). This finding indicates that the direct dehydrogenation of propane plays an important role in the oxidative dehydrogenation of propane over supported vanadium catalysts, especially at higher reaction temperatures.

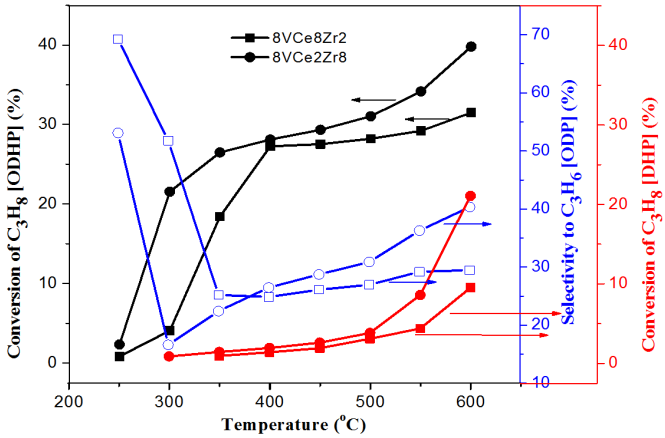

Figure 15. Conversion of C_3H_8 in ODHP, selectivity to C_3H_6 in ODHP and conversion of C_3H_8 in DHP as a function of the temperature of the reaction of the 8VCe8Zr2 and 8VCe2Zr8 catalysts

The results of the DR UV-vis, Raman, H_2-TPR and XPS studies indicate that the different Ce/Zr ratios of supports make a great difference on the formation of the VO_x species on the $Ce_xZr_{1-x}O_2$ catalyst surface. The polymeric surface vanadium species of 8VCe2Zr8 are greater than those of 8VCe8Zr2. In combination with the results of the catalytic performance, we suggest that the catalysts with polymerized VO_x species are more strongly oxidizing toward CO and less selective for propylene than the catalysts with isolated VO_x species in the ODHP. Furthermore, the polyvanadate species show high activity to the direct dehydrogenation of propane. These results agree with the previous reports about the ODHP using vanadia catalysts, indicating that the isolated vanadate species were significantly less active than polyvanadate[54]. However, there have been several different ideas about the active species on the catalytic dehydrogenation of n-butane over a VO_x-based catalyst. Jackson *et al.*[51] proposed that the reduced polyvanadate species are the optimum compounds for dehydrogenation reaction, whereas McGregor and coworkers[57] identified the isolated vanadia species as the active compounds for the dehydrogenation of butane. The recent work on the nature of active phase of VO_x catalysts supported on a SiBeta zeolite for dehydrogenation reaction of propane to propylene also suggested that the aggregation degree of VO_x species determined the deactivation rate and propylene selectivity[26].

3.2.3 Catalyst stability in the oxidative dehydrogenation of propane

DHP is a highly endothermic equilibrium limited reaction that is generally carried out at a proper atmospheric pressure and relatively high temperatures. Catalytic deactivation may be induced by the high temperatures required to achieve a sensible propane conversion for the dehydrogenation reaction. The VO_x-based catalysts in DHP suffer from two typical deactivation types: (i) coke deposition, a reversible deactivation and (ii) the changes of the active V phases, an irreversible deactivation[50]. The DHP reaction operated over mesoporous nanostructured $VO_x/Ce_xZr_{1-x}O_2$ catalysts in the ODHP at higher temperatures. Thus, in order to understand the catalytic behavior of the prepared catalysts, time-on-stream studies were carried out. **Figure 16** exhibits

the catalytic performance of the 8VCe2Zr8 catalyst in an 80 h at 450 °C. The steady-state values of ca. 24% for the conversion of propane, of ca. 32% for the selectivity to propylene and of ca. 6% for the propylene yield were obtained during the experiment. The good stability of 8VCe2Zr8 in the OHDP, feeding oxygen as well as the propane, indicates that this alternative process is energetically favorable on account of the lower required temperatures and the sequential enhanced catalytic stability by the prevention of coke deposition. Furthermore, this reaction is neither endothermic nor equilibrium limited and therefore provides important advantages compared to DHP processes.

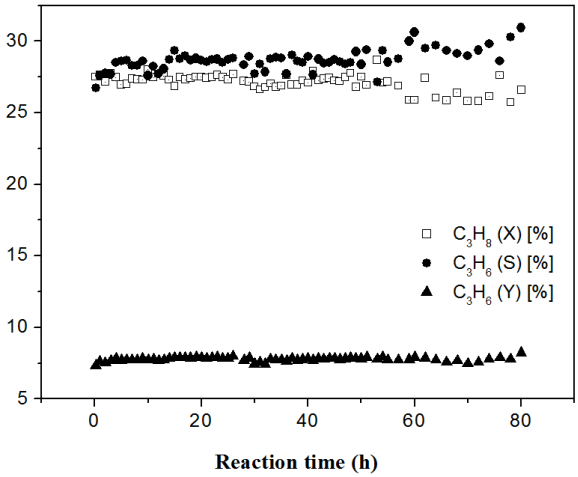

Figure 16. Variation in the conversion of C_3H_8, selectivity to C_3H_6 and yield of C_3H_6 with time-on-stream over 8VCe2Zr8 in the ODHP at 450 °C

Figure 17a shows the Raman spectra of the 8VCe2Zr8 catalyst after 80 h on stream under C_3H_8-O_2 conditions. The Raman spectra are similar for the used and fresh samples. The Raman bands of the catalyst do not disappear after the reaction, indicating that the deposited hydrocarbons do not appear on the surface of the catalyst[56]. Furthermore, no new bands appear in the spectra. For the DR UV-vis study, over time, the absorbance increases, if the absorbance between 600 and 800 nm are corresponding to the coke formation[18]. However, the DR UV-vis spectra of the used and fresh catalysts are very similar (**Figure 17b**), suggesting that the mesoporous nanostructured 8VCe2Zr8 catalyst present a stable catalytic performance in the oxidative dehydrogenation of propane.

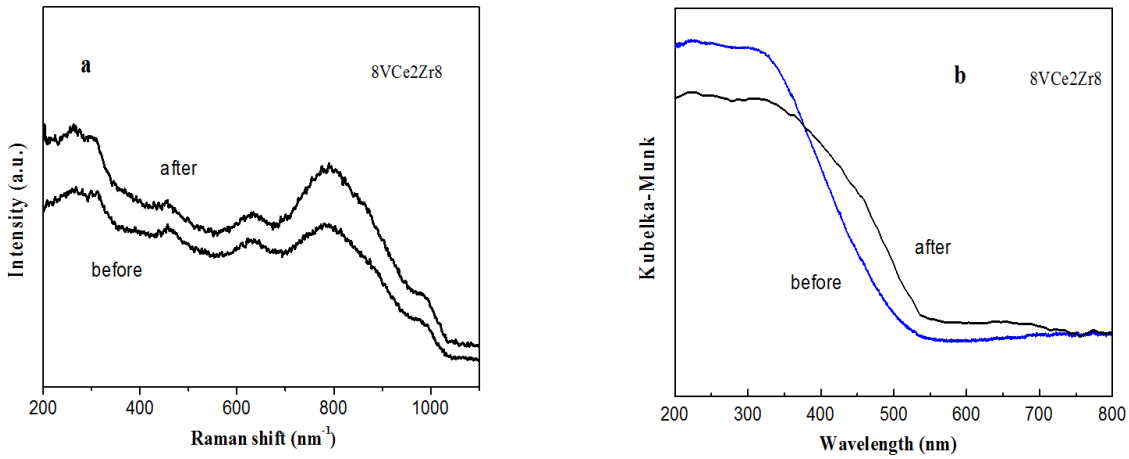

Figure 17. (a) Raman spectra of the fresh and used 8VCe2Zr8 catalysts; (b) Diffuse reflectance UV-vis spectra of the fresh and used 8VCe2Zr8 catalysts

4. Conclusions

By the approach of a surfactant-assisted method of nanoparticle assembly, mesoporous nanostructured $VO_x/Ce_xZr_{1-x}O_2$ catalysts with narrow mesopore size distributions and high surface areas were successfully synthesized. The $CeVO_4$ phase contained in the catalysts with excessive VO_x content (> 10%) or calcined at high temperatures (> 650 °C), has negative influence on the catalytic performance of the ODHP reaction. The results of the H_2-TPR, Raman, DR XPS and UV-vis studies indicate that different Ce/Zr ratios of the supports influenced the formation of VO_x species on the $Ce_xZr_{1-x}O_2$ surface. Detailedly, adding ZrO_2 to CeO_2 lattice to form solid solution is conducive to the release of bulk lattice oxygen, boosting the ODHP reaction. The polymeric surface vanadium species with relatively low catalytic activity are greater on/in 8VCe2Zr8 than on/in 8Vce8Zr2, determined by XRD and H_2-TPR. The existence of V-O-V and V-O-Zr bonds which are identified as highly reactive sites[58] are detected via UV-vis spectroscopy on the 8VCe8Zr2 and 8VCe2Zr8 catalysts with no obvious V = O bonds, causing the higher catalytic activity of these catalysts compared to other $VO_x/Ce_xZr_{1-x}O_2$ catalysts. In combination with the results of the catalytic performance, it is suggested that the catalysts with polymerized VO_x species are more strongly oxidizing toward CO and less selective for propylene than the catalysts with isolated VO_x species in the ODHP. Furthermore, the polyvanadate species show high activity to the direct dehydrogenation of propane. The 8VCe2Zr8 catalyst exhibits a stable catalytic performance in the oxidative dehydrogenation of propane.

Acknowledgements

This work was supported by the State Key Laboratory of Catalytic Materials and Reaction Engineering (RIPP, SINOPEC), and the Fundamental Research Funds for the Inner Mongolia Normal University (2022JBQN085).

References

[1] Hu ZP, Yang D, Wang Z, *et al*. State-of-the-art catalysts for direct dehydrogenation of propane to propylene. *Chinese Journal of Catalysis*, 2019;40(9):1233-1254. https://doi.org/10.1016/S1872-2067(19)63360-7

[2] Hu P, Lang WZ, Yan X, *et al*. Influence of gelation and calcination temperature on the structure-performance of porous VO_x-SiO_2 solids in non-oxidative propane dehydrogenation. *Journal of Catalysis*, 2018;358:108-117. https://doi.org/10.1016/j.jcat.2017.12.004

[3] Hu ZP, Wang Z and Yuan ZY. Cr/Al_2O_3 catalysts with strong metal-support interactions for stable catalytic dehydrogenation of propane to propylene. *Molecular Catalysis*, 2020;493:111052. https://doi.org/10.1016/j.mcat.2020.111052

[4] Otroshchenko TP, Rodemerck U, Linke D, *et al*. Synergy effect between Zr and Cr active sites in binary $CrZrO_x$ or supported $CrO_x/LaZrO_x$: consequences for catalyst activity, selectivity and durability in non-oxidative propane dehydrogenation. *Journal of Catalysis*, 2017;356:197-205. https://doi.org/10.1016/j.jcat.2017.10.012

[5] Chen C, Hu Z, Zhang S, *et al*. Advance in the catalysts of direct dehydrogenation of propane to propylene. *Acta Petrolei Sinica (Petroleum Processing Section)*, 2020;36(3):639-652. https://doi.org/10.3969/j.issn.1001-8719.2020.03.025

[6] De Rossi S, Ferraris G, Fremiotti S, *et a*l. Isobutane dehydrogenation on chromia/zirconia catalysts. *Applied Catalysis A: General*, 1993;106(1):125-141. https://doi.org/10.1016/0926-860X(93)80160-R

[7] De Rossi S, Casaletto MP, Ferraris G, *et al*. Chromia/zirconia catalysts with Cr content exceeding the monolayer. A comparison with chromia/alumina and chromia/silica for isobutane dehydrogenation. *Applied Catalysis A: General*, 1998;167(2):257-270. https://doi.org/10.1016/S0926-860X(97)00315-3

[8] Cavani F, Ballarini N and Cericola A. Oxidative dehydrogenation of ethane and propane: how far from commercial implementation?. *Catalysis Today*, 2007;127(1-4):113-131. https://doi.org/10.1016/j.cattod.2007.05.009

[9] Hess C. Direct correlation of the dispersion and structure in vanadium oxide supported on silica SBA-15. *Journal of Catalysis*, 2007;248(1):120-123. https://doi.org/10.1016/j.jcat.2007.02.024

[10] Grzybowska B, Mekšs P, Grabowski R, *et al*. Effect of potassium addition to V_2O_5/TiO_2 and

MoO_3/TiO_2 catalysts on their physicochemical and catalytic properties in oxidative dehydrogenation of propane. *Studies in Surface Science and Catalysis*, 1994;82:151-158. https://doi.org/10.1016/S0167-2991(08)63407-2

[11] Grabowski R, Grzybowska B, Samson K, *et al*. Effect of alkaline promoters on catalytic activity of V_2O_5/TiO_2 and MoO_3/TiO_2 catalysts in oxidative dehydrogenation of propane and in isopropanol decomposition. *Applied Catalysis A: General*, 1995;125(1):129-144. https://doi.org/10.1016/0926-860X(94)00274-6

[12] Blasco T and Nieto JML. Oxidative dyhydrogenation of short chain alkanes on supported vanadium oxide catalysts. *Applied Catalysis A: General*, 1997;157(1-2):117-142. https://doi.org/10.1016/S0926-860X(97)00029-X

[13] Klisińska A, Samson K, Gressel I, *et al*. Effect of additives on properties of V_2O_5/SiO_2 and V_2O_5/MgO catalysts: I. Oxidative dehydrogenation of propane and ethane. *Applied Catalysis A: General*, 2006;309(1):10-16. https://doi.org/10.1016/j.apcata.2006.04.028

[14] Vedyagin AA, Mishakov IV and Ilyina EV. A step forward in the preparation of V–Mg–O catalysts for oxidative dehydrogenation of propane. *Journal of Sol-Gel Science and Technology*, 2021;97(1):117-125. https://doi.org/10.1007/s10971-020-05438-1

[15] Mishakov IV, Vedyagin A, Bedilo AF, *et a*l. Aerogel VO_x/MgO catalysts for oxidative dehydrogenation of propane. *Catalysis Today*, 2009;144(3-4):278-284. https://doi.org/10.1016/j.cattod.2009.01.018

[16] Kondratenko EV and Baerns M. Catalytic oxidative dehydrogenation of propane in the presence of O_2 and N_2O-the role of vanadia distribution and oxidant activation. *Applied Catalysis A: General*, 2001;222(1-2):133-143. https://doi.org/10.1016/S0926-860X(01)00836-5

[17] Kondratenko EV, Cherian M, Baerns M, *et al*. Oxidative dehydrogenation of propane over V/MCM-41 catalysts: comparison of O_2 and N_2O as oxidants. *Journal of Catalysis*, 2005;234(1):131-142. https://doi.org/10.1016/j.jcat.2005.05.025

[18] Kondratenko EV, Ovsitser O, Radnik J, *et al*. Influence of reaction conditions on catalyst composition and selective/non-selective reaction pathways of the ODP reaction over V_2O_3, VO_2 and V_2O_5 with O_2 and N_2O. *Applied Catalysis A: General*, 2007;319:98-110. https://doi.org/10.1016/j.apcata.2006.11.021

[19] Michorczyk P and Ogonowski J. Dehydrogenation of propane to propene over gallium oxide in the presence of CO_2. *Applied Catalysis A: General*, 2003;251(2):425-433. https://doi.org/10.1016/S0926-860X(03)00368-5

[20] Frank B, Dinse A, Ovsitser O, *et al*. Mass and heat transfer effects on the oxidative dehydrogenation of propane (ODP) over a low loaded VO_x/Al_2O_3 catalyst. *Applied Catalysis A: General*, 2007;323:66-76. https://doi.org/10.1016/j.apcata.2007.02.006

[21] Gao X, Xin Q and Guo X. Support effects on magnesium-vanadium mixed oxides in the oxidative dehydrogenation of propane. *Applied Catalysis A: General*, 1994;114(2):197-205. https://doi.org/10.1016/0926-860X(94)80173-8

[22] Watling TC, Deo G, Seshan K, *et al*. Oxidative dehydrogenation of propane over niobia supported vanadium oxide catalysts. *Catalysis Today*, 1996;28(1-2):139-145. https://doi.org/10.1016/0920-5861(95)00221-9

[23] Blasco T, Galli A, Nieto JML, *et al*. Oxidative dehydrogenation of ethane andn-butane on VO_x/Al_2O_3 catalysts. *Journal of Catalysis*, 1997;169(1):203-211. https://doi.org/10.1006/jcat.1997.1673

[24] Khodakov A, Olthof B, Bell AT, *et al*. Structure and catalytic properties of supported vanadium oxides: support effects on oxidative dehydrogenation reactions. *Journal of Catalysis*, 1999;181(2): 205-216. https://doi.org/10.1006/jcat.1998.2295

[25] Lemonidou AA, Nalbandian L and Vasalos IA. Oxidative dehydrogenation of propane over vanadium oxide based catalysts: effect of support and alkali promoter. *Catalysis Today,* 2000;61(1-4):333-341. https://doi.org/10.1016/S0920-5861(00)00393-X

[26] Chen C, Sun M, Hu Z, *et al*. Nature of active phase of VO_x catalysts supported on SiBeta for direct dehydrogenation of propane to propylene. *Chinese Journal of Catalysis*, 2020;41(2):276-285.

https://doi.org/10.1016/S1872-2067(19)63444-3

[27] Reina TR, Ivanova S, Idakiev V, *et al*. Nanogold mesoporous iron promoted ceria catalysts for total and preferential CO oxidation reactions. *Journal of Molecular Catalysis A: Chemical*, 2016;414: 62-71. https://doi.org/10.1016/j.molcata.2016.01.003

[28] Wang S, Xu X, Xiao P, *et a*l. Cooperative effect between copper species and oxygen vacancy in $Ce_{0.7-x}Zr_xCu_{0.3}O_2$ catalysts for carbon monoxide oxidation. *Frontiers of Chemical Science and Engineering*, 2021;15(6):1524-1536. https://doi.org/10.1007/s11705-021-2106-2

[29] Kang M, Song MW and Lee CH. Catalytic carbon monoxide oxidation over CoO_x/CeO_2 composite catalysts. *Applied Catalysis A: General*, 2003;251(1):143-156. https://doi.org/10.1016/S0926-860X(03)00324-7

[30] Kim TH, Kang KH, Baek M, *et al*. Dehydrogenation of propane to propylene with lattice oxygen over $CrOy/Al_2O_3$-ZrO_2 catalysts. *Molecular Catalysis*, 2017;433:1-7. https://doi.org/10.1016/j.mcat.2016.12.004

[31] Kim TH, Gim MY, Song JH, *et al*. Deactivation behavior of CrO_y/Al_2O_3-ZrO_2 catalysts in the dehydrogenation of propane to propylene by lattice oxygen. *Catalysis Communications*, 2017;97: 37-41. https://doi.org/10.1016/j.catcom.2017.04.016

[32] Cao JL, Wang Y, Zhang TY, *et a*l. Preparation, characterization and catalytic behavior of nanostructured mesoporous $CuO/Ce_{0.8}Zr_{0.2}O_2$ catalysts for low-temperature CO oxidation. *Applied Catalysis B: Environmental*, 2008;78(1-2):120-128. https://doi.org/10.1016/j.apcatb.2007.09.007

[33] Chen YZ, Liaw BJ and Chen HC. Selective oxidation of CO in excess hydrogen over CuO/ $Ce_xZr_{1-x}O_2$ catalysts. *International Journal of Hydrogen Energy*, 2006;31(3):427-435. https://doi.org/10.1016/j.ijhydene.2005.11.004

[34] Deng QF, Ren TZ, Agula B, *et al*. Mesoporous $Ce_xZr_{1-x}O_2$ solid solutions supported CuO nanocatalysts for toluene total oxidation. *Journal of Industrial and Engineering Chemistry,* 2014;20(5):3303-3312. https://doi.org/10.1016/j.jiec.2013.12.012

[35] Daniell W, Ponchel A, Kuba S, *et al*. Characterization and catalytic behavior of VO_x-CeO_2 catalysts for the oxidative dehydrogenation of propane. *Topics in Catalysis,* 2002;20(1):65-74. https://doi.org/10.1023/A:1016399315511

[36] Martınez-Huerta MV, Coronado JM, Fernández-Garcıa M, et al. Nature of the vanadia–ceria interface in V5+/CeO_2 catalysts and its relevance for the solid-state reaction toward $CeVO_4$ and catalytic properties. *Journal of Catalysis*, 2004;225(1):240-248. https://doi.org/10.1016/j.jcat.2004.04.005

[37] Heracleous E, Machli M, Lemonidou AA, *et a*l. Oxidative dehydrogenation of ethane and propane over vanadia and molybdena supported catalysts. *Journal of Molecular Catalysis A: Chemical*, 2005;232(1-2):29-39. https://doi.org/10.1016/j.molcata.2005.01.027

[38] Postole G, Chowdhury B, Karmakar B, *et al*. Knoevenagel condensation reaction over acid–base bifunctional nanocrystalline $Ce_xZr_{1-x}O_2$ solid solutions. J*ournal of Catalysis*, 2010;269(1): 110-121. https://doi.org/10.1016/j.jcat.2009.10.022

[39] Pijolat M, Valdivieso F, Vidal H, *et al*. Surface and structural characterization of $Ce_xZr_{1-x}O_2$ CEZIRENCAT mixed oxides as potential three-way catalyst promoters. *Journal of the Chemical Society, Faraday Transactions*, 1998;94(24): 3717-3726. https://doi.org/10.1039/A807680D

[40] Reddy BM, Khan A, Yamada Y, *et al*. Structural characterization of CeO_2-MO_2 (M = Si^{4+}, Ti^{4+}, and Zr^{4+}) mixed oxides by Raman spectroscopy, X-ray photoelectron spectroscopy, and other techniques. *The Journal of Physical Chemistry B*, 2003;107(41):11475-11484. https://doi.org/10.1021/jp0358376

[41] Idakiev V, Dimitrov D, Tabakova T, *et al.* Catalytic abatement of CO and volatile organic compounds in waste gases by gold catalysts supported on ceria-modified mesoporous titania and zirconia. *Chinese Journal of Catalysis*, 2015;36(4):579-587. https://doi.org/10.1016/S1872-2067(14)60283-7

[42] Gao LJ, Chen L, Ren JT, *et al.* Mesoporous $Cd_xZn_{1-x}S$ with abundant surface defects for efficient photocatalytic hydrogen production. *Journal of Colloid and Interface Science*, 2021;589:25-33. https://doi.org/10.1016/j.jcis.2020.12.112

[43] Serrano-Ruiz JC, Luettich J, Sepúlveda-Escribano A, *et al.* Effect of the support composition on the vapor-phase hydrogenation of crotonaldehyde over Pt/$Ce_xZr_{1-x}O_2$ catalysts. *Journal of Catalysis*, 2006;241(1):45-55. https://doi.org/10.1016/j.jcat.2006.04.006

[44] Pokrovski KA and Bell AT. An investigation of the factors influencing the activity of Cu/$Ce_xZr_{1-x}O_2$ for methanol synthesis via CO hydrogenation. *Journal of Catalysis*, 2006;241(2):276-286. https://doi.org/10.1016/j.jcat.2006.05.002

[45] Machold T, Suprun WY and Papp H. Characterization of VO_x-TiO_2 catalysts and their activity in the partial oxidation of methyl ethyl ketone. *Journal of Molecular Catalysis A: Chemical*, 2008;280(1-2):122-130. https://doi.org/10.1016/j.molcata.2007.11.001

[46] Kanervo JM, Harlin ME, Krause AOI, *et al*. Characterisation of alumina-supported vanadium oxide catalysts by kinetic analysis of H_2-TPR data. *Catalysis Today*, 2003;78(1-4):171-180. https://doi.org/10.1016/S0920-5861(02)00326-7

[47] Koranne MM, Goodwin JG and Marcelin G. Characterization of silica-and alumina-supported vanadia catalysts using temperature programmed reduction. *Journal of Catalysis*, 1994;148(1):369-377. https://doi.org/10.1006/jcat.1994.1217

[48] Varma S, Wani BN and Gupta N M. Synthesis, characterization, and redox behavior of mixed orthovanadates $La_{1-x}Ce_xVO_4$. *Materials Research Bulletin*, 2002;37(13):2117-2127. https://doi.org/10.1016/S0025-5408(02)00888-7

[49] Gazzoli D, De Rossi S, Ferraris G, *et al*. Bulk and surface structures of V_2O_5/ZrO_2 catalysts for n-butane oxidative dehydrogenation. *Journal of Molecular Catalysis A: Chemical*, 2009;310(1-2):17-23. https://doi.org/10.1016/j.molcata.2009.05.014

[50] Zhang H, Liu Z, Feng Z, *et al*. Effective silica supported Sb-V mixed oxide catalyst for selective oxidation of methanol to formaldehyde. *Journal of Catalysis*, 2008;260(2):295-304. https://doi.org/10.1016/j.jcat.2008.09.019

[51] Jackson SD and Rugmini S. Dehydrogenation of n-butane over vanadia catalysts supported on θ-alumina. *Journal of Catalysis*, 2007;251(1):59-68. https://doi.org/10.1016/j.jcat.2007.07.015

[52] Liu YM, Cao Y, Yi N, *et al*. Vanadium oxide supported on mesoporous SBA-15 as highly selective catalysts in the oxidative dehydrogenation of propane. *Journal of Catalysis*, 2004;224(2):417-428. https://doi.org/10.1016/j.jcat.2004.03.010

[53] Tian H, Ross EI and Wachs IE. Quantitative determination of the speciation of surface vanadium oxides and their catalytic activity. *The Journal of Physical Chemistry B*, 2006;110(19):9593-9600. https://doi.org/10.1021/jp055767y

[54] Klose F, Wolff T, Lorenz H, *et al*. Active species on γ-alumina-supported vanadia catalysts: nature and reducibility. *Journal of Catalysis*, 2007;247(2):176-193. https://doi.org/10.1016/j.jcat.2007.01.013

[55] Wang G, Dai H, Zhang L, *et al*. CrOx/nano-$Ce_{0.60}Zr_{0.35}Y_{0.05}O_2$ catalysts that are highly selective for the oxidative dehydrogenation of isobutane to isobutene. *Applied Catalysis A: General*, 2010;375(2):272-278. https://doi.org/10.1016/j.apcata.2010.01.005

[56] Dinse A, Frank B, Hess C, *et al*. Oxidative dehydrogenation of propane over low-loaded vanadia catalysts: Impact of the support material on kinetics and selectivity. *Journal of Molecular Catalysis A: Chemical*, 2008;289(1-2):28-37. https://doi.org/10.1016/j.molcata.2008.04.007

[57] McGregor J, Huang Z, Shiko G, *et al.* The role of surface vanadia species in butane dehydrogenation over VO_x/Al_2O_3. *Catalysis Today*, 2009;142(3-4):143-151. https://doi.org/10.1016/j.cattod.2008.07.022

[58] Ternero-Hidalgo JJ, Daturi M, Clet G, *et al*. A simultaneous operando FTIR & Raman study of propane ODH mechanism over V-Zr-O catalysts. *Catalysis Today*, 2022;387:197-206. https://doi.org/10.1016/j.cattod.2021.06.012